Journal of Nanobiotechnology

RESEARCH

Open Access

ACYP2 functions as an innovative nano-therapeutic target to impede the progression of hepatocellular carcinoma by inhibiting the activity of TERT and the KCNN4/ERK pathway

Yixuan Wu[1,2†], Hongyi Bao[1,2†], Jinran Wu[1,2†], Bairong Chen[1,2], Jing Xu[1,2], Kangfeng Jin[1,2], Lin Chen[3*], Guang Zhu[4*] and Feng Wang[1,2*]

Abstract

An increasing body of evidence suggests that acylphosphatase-2 (ACYP2) polymorphisms are correlated with an increased susceptibility to a range of malignancies. Nevertheless, its potential functions, molecular mechanisms in hepatocellular carcinoma (HCC) and whether it can be act as a therapeutic target remain uninvestigated. Herein, ACYP2 was found to be lowly expressed in HCC and was negatively correlated with tumor size, tumor differentiation, microvascular invasion and the prognosis of HCC patients. Functional investigations revealed that overexpression of ACYP2 inhibited the proliferation and metastasis of HCC cells while promoting apoptosis; knockdown of ACYP2 had the exact opposite effect. Additionally, it was observed that ACYP2 was distributed in both the cytoplasm and nucleus of HCC cells. According to the mechanistic studies, the expression of potassium calcium-activated channel subfamily N member 4 (KCNN4) was negatively regulated by cytoplasmic ACYP2, resulting in the inhibition of K^+ outflow and subsequent inactivation of the ERK pathway, which impeded the growth and metastasis of HCC. Furthermore, the activity of telomerase reverse transcriptase (TERT) was inhibited by nuclear ACYP2, leading to the reduction in length of telomeres and consequent reversal of HCC cell immortalization. Additionally, a novel targeted nanotherapy strategy was developed wherein the pcDNA-ACYP2 vector was encapsulated within polyetherimide nanoparticles (PEI/NPs), which were subsequently coated with HCC cell membranes (namely pcDNA/PEI/NPs@M). Safety and targeting characteristics abound for these nanocomposites, in both subcutaneous graft tumor models and orthotopic mouse models, they inhibited the progression of HCC by impeding TERT activity and the KCNN4/ERK pathway. In conclusion, our research identifies novel molecular mechanisms involving cytoplasmic and nuclear ACYP2 that inhibit the progression of HCC. Moreover, pcDNA/PEI/NPs@M represents a targeted therapeutic strategy for HCC that holds great promising.

†Yixuan Wu, Hongyi Bao and Jinran Wu contributed equally to this work.

*Correspondence:
Lin Chen
xiaobei227@sina.com
Guang Zhu
gzhu@ust.hk
Feng Wang
richardwangf@163.com
Full list of author information is available at the end of the article

Keywords Hepatocellular carcinoma, ACYP2, KCNN4, TERT, Nanotherapy

Graphical Abstract

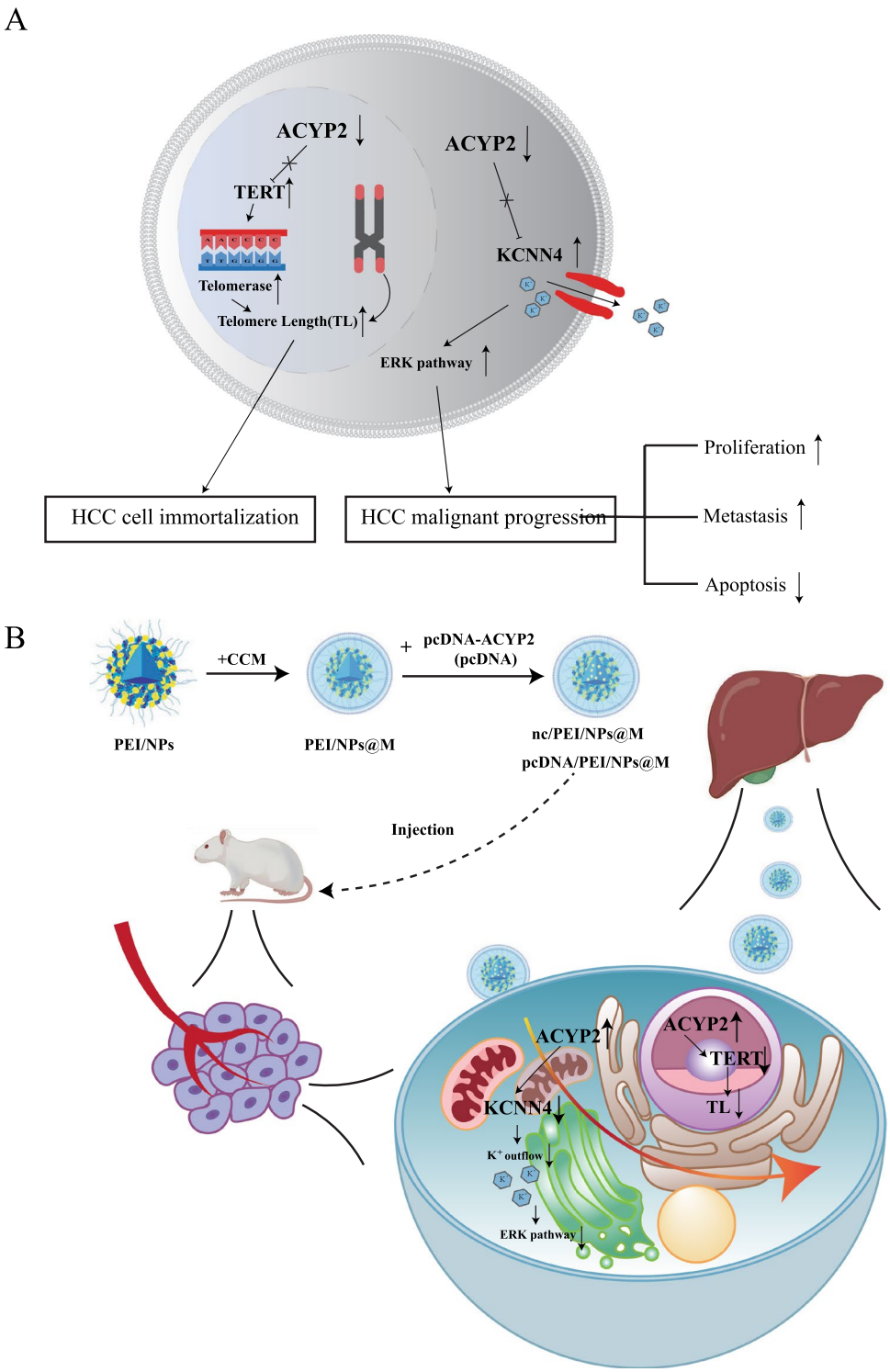

Introduction

Hepatocellular Carcinoma (HCC) is the most prevalent form of liver cancer and the second leading cause of cancer-related mortality globally. It is categorized as one of the most preponderant malignancies [1]. During the initial phases of HCC, symptoms are not conspicuous, leading to the diagnosis of more than 60% of patients at an advanced stage, thereby substantially reducing their 5-year survival rate. Furthermore, the absence of efficacious treatment modalities frequently renders punctual intervention unattainable for patients afflicted with advanced HCC [2]. This necessitates an immediate investigation into precise biomarkers for early detection and the identification of more effective therapeutic targets for this fatal disease.

Acylphosphatase-2 (ACYP2), an isoform of ACYP, is extensively distributed in vertebrate tissues and is located at chromosome 2p16.2 [3]. It is one of the enzymes that has been identified thus far with the smallest molecular weight. Its specific function is to facilitate the hydrolysis of acylphosphate compounds in vitro. ACYP1 and ACYP2 are isoforms that consist of 60% identical sequence and display identical substrate specificity. Research has shown that ACYP is involved in numerous vital biological processes in vertebrates, including regulation of the glycolytic pathway, induction of apoptosis, and regulation of Na^+, K^+, and Ca^{2+} ion transporters [4, 5]. Furthermore, it has been documented that ACYP2 polymorphisms are correlated with an increased susceptibility to a range of malignancies, such as gastrointestinal cancer, renal cell cancer, and squamous carcinoma of the larynx [6, 7]. Li et al. [8] showed that ACYP2 is closely associated with gliomas. Except for this, the expression mechanism of ACYP2 in other cancers is not clear. Based on these results, it appears that ACYP2 can play a role in the formation and progression of the vast majority of cancers. Nonetheless, the precise functions of ACYP2 in HCC carcinogenesis require additional investigation.

Potassium calcium-activated channel subfamily N (KCNN), a Ca^{2+}-dependent potassium channel is encoded by four distinct genes (KCNN1–4), the expression of which is regulated in a manner that is specific to progression, development and tissue, which plays an important role as a key biomarker in a variety of biological processes [9, 10]. However, although a large number of studies on KCNN expression have been conducted, the specific mechanisms of its role in HCC are still not fully understood.

An increasing body of evidence supports the notion that nonviral vector-mediated gene delivery offers a viable strategy for effective gene transfer owing to its enhanced biosafety, diminished likelihood of detrimental immune responses, and capacity to integrate viral genes into the genome of the host [11]. The utilization of nanoparticles (NPs) in the development of gene-drug delivery systems has become increasingly prevalent in recent times [12]. NPs fail to progress to the clinical stage on account of their toxicity and degradation [13]. Increasing the biocompatibility of materials is necessary to surmount these obstacles and enhance the implementation of NPs. Cationic polyethyleneimine (PEI) is a substance utilized in the delivery of nucleic acids [14]. PEI and its derivatives are extensively utilized as reference agents in the field of polymer-based gene delivery and in fundamental investigations [15]. As a result, PEI was employed in conjunction with NPs to enhance the therapeutic impact [16]. Furthermore, the encapsulation of nonviral vector-mediated gene delivery systems in nanomaterials coated with tumor cell membranes can prevent unanticipated losses during transport to the target site, enabling effective local gene therapy while minimizing nonspecific diffusion into other tissues [17, 18]. However, additional research is necessary to ascertain whether the treatment is more effective with the PEI/NPs encapsulating the vector coated with HCC cell membrane.

The present study documented a notable reduction in the expression of ACYP2 in HCC. Furthermore, it was observed that cytoplasmic ACYP2 inhibited the ERK pathway by negatively regulating potassium calcium-activated channel subfamily N member 4 (KCNN4), thereby effectively impeding K^+ efflux and thereby inhibiting tumor growth and metastasis in HCC cells. Furthermore, through its regulation of telomerase reverse transcriptase (TERT) activity, nuclear ACYP2 may possess the ability to halt the immortalization process of HCC cells by inducing telomere shortening. Furthermore, the pcDNA-ACYP2 vector was encapsulated within PEI/NPs nanomaterials and subsequently coated with the HCC cell membrane to create the pcDNA/PEI/NPs@M nanocomposites. These nanocomposites demonstrated remarkable inhibitory effects on the development of orthotopic HCC in mouse models. These results indicate that ACYP2, in its capacity as a tumor suppressor, may have therapeutic potential as a target for HCC.

Materials and methods

Clinical sample

Fifty-two HCC tissues and their corresponding adjacent normal tissues were collected at the Affiliated Hospital of Nantong University between May 2018 and May 2020. A pathological examination was performed on each tissue prior to its storage at −80 °C for subsequent analysis. Before undergoing surgery, none of the patients had been administered chemotherapy or radiation therapy. The ethics committee of the Affiliated Hospital of Nantong University approved this research, and informed

consent was obtained from all participants. In Table S1, the clinicopathological characteristics of the HCC cases are detailed.

RNA extraction, reverse transcription, and qRT-PCR

QRT-PCR, RNA extraction, and reverse transcription Total RNA was reverse-transcribed into cDNA using a reverse transcription kit (Thermo Fisher Scientific, USA) after being extracted with TRIzol reagent (Invitrogen, USA). The cDNAs were amplified using a Plus SYBR real-time PCR mixture (BioTeke, Beijing, China) on a Light Cycler 480 instrument (Roche, Germany). Comparative cycle threshold values ($2^{-\Delta\Delta Ct}$) were computed in order to assess the expression levels of ACYP2, KCNN4, and TERT. The reference gene for ACYP2, KCNN4, and TERT was GAPDH. The comprehensive primer specifications are detailed in Table S2.

Cell culture

Human HCC cell lines and LO2, a normal liver cell line, were supplied for cell culture by the Cell Bank of the Chinese Academy of Sciences (Shanghai, China). LO2 cells were cultured in RPMI-1640 medium (Corning, NY, USA), while HCC cells were cultured in Dulbecco's modified Eagle's medium (DMEM, Corning, USA). 10% fetal bovine serum (FBS, Lonsera, USA) was added to each cell in a humidified environment with 5% CO_2 and 37 °C.

Cell transfection

HCC cells were subjected to transfection with various constructs, including si-ACYP2 (si-ACYP2-1, si-ACYP2-2), siRNA negative control (si-NC), pcDNA negative control (vector), and pcDNA-ACYP2. Using Lipofectamine 3000 (Invitrogen, USA), the cells were transfected when confluence had approximated 70%. The qRT-PCR assay was utilized to evaluate the transfection efficiency following a 48-h incubation period. For a summary of the siRNA vectors used in this investigation, see Table S3.

Cell proliferation

For the cell proliferation assay, the CCK-8 reagent (MedChemExpress, Shanghai, China) was utilized. In 96-well plates, HCC cells were seeded at a density of 3000 cells per well. Each well was supplemented with 10 μL of CCK-8 solution at 24, 48 and 72 h post-inoculation; incubation was then continued for an additional 2 h. The absorbance values were subsequently determined using a microplate reader (Thermo Fisher Scientific, USA) at a wavelength of 450 nm. Furthermore, an evaluation of cell proliferation was performed utilizing the EdU cell proliferation assay reagent manufactured by Beyotim, China. HCC cells were incubated in 48-well plates containing 100 μL of EdU working solution for a duration of 2 h. The cells were then immersed for 15 min in a 4% solution of paraformaldehyde before being encapsulated in a PBS solution supplemented with 3% bovine serum albumin (BSA). Following a 15-min immersion in a 0.3% Triton X-100 solution, the cells were subjected to a subsequent 15-min staining step using Hoechst 33258 stain solution at a concentration of 1 μg/mL. In conclusion, a fluorescent microscope (Olympus Corporation, Japan) was utilized to examine the cells.

Clone formation assay

In order to conduct the clone formation assay, an approximate density of 1×10^3 HCC cells were seeded per well into six-well plates, followed by a 2-week incubation period. Following that, the cells were fixed using a formaldehyde solution containing 4% and subsequently stained using a crystal violet solution containing 0.1%. Positive clones are observed using a microscope. These clones are usually aggregates containing more than 50 cells each. Clones are usually between 0.3 and 1.0 mm in size. The positive clones are photo documented under the microscope using a camera. Positive cells were counted and analyzed using imageJ.

Wound-healing assay

For the wound-healing assay, the back of the six-well cell culture plates was annotated with a marker pen. Subsequently, cells were inoculated into each well in a manner that ensured the inoculation fusion rate could attain 100% as a monolayer during the overnight period. Several uniformly spaced incisions were made with a 200-μL pipette tip positioned perpendicular to the culture plates, once the cells had completely covered the lower surfaces. Following the removal of cell fragments caused by the scratch, the cells were washed three times with PBS buffer and the cell culture solution was drained off. Each well was supplemented with serum-free medium, and the culture plates were incubated at 37 °C in an incubator containing 5% CO_2. Following this, photographs were captured at 0 h and notes were made at 24 h, respectively. The recovery rate of the abrasion was assessed and computed utilizing ImageJ software in conjunction with the gathered images.

Cell invasion assays

In order to conduct cell invasion assays, the upper chamber was inoculated with 7×10^5 cells/mL of HCC cells in serum-free DMEM medium and positioned in a 100 μL Matrigel (1:10, BD Bioscience). In order to supplement the lower chambers, DMEM containing 10% FBS was added. The compartments were extracted following a 48-h incubation period, followed by fixation in a 4%

solution of paraformaldehyde and staining with a 0.1%ssa solution of crystal violet. Following a gentle wiping of the upper chambers with a cotton swab, the quantity of invading cells in the lower chambers was determined using a microscope. Cell counting was performed with imageJ using the Multi-Point tool, and positive cells were counted and analyzed.

Cell apoptosis experiment

For the cell apoptosis experiment, 70% ethanol was used to stabilize HCC cells that were collected. After adding 50 μL of enzyme solution, the mixture was incubated at 37 °C. Following that, the cells were stained with 200 μL of Annexin V-Alexa Fluor 647/PI-containing dye (Beyotime, China) under dark conditions and incubated on ice. Flow cytometry was subsequently employed to analyze apoptotic cells (BD Bioscience, USA).

Nuclear and cytoplasmic RNA extraction

Extraction from the nucleus and cytoplasmic RNA was performed utilizing nuclear and cytoplasmic protein extraction kits, manufactured by Beyotime Biotechnology. An qRT-PCR assay was subsequently utilized to determine the level of ACYP2 expression in the cytoplasm and nucleus. (18s serves as the nuclear reference control, while U6 serves as the cytoplasmic reference control).

Confocal microscope assay

In order to perform a confocal microscope assay utilizing immunofluorescence, the cells were cultured overnight on a coverslip, fixed for 3 min with 30% paraformaldehyde, and subsequently stained with DAPI (1 μg/mL). To perform PBFI AM (K^+ Indicator) staining, cells were subjected to a 1:400 dilution of PBFI AM (K^+ Indicator) and incubated for 4 h with equivalent volumes of Pluronic F-127 (Maokangbio, China). The cells were subsequently rinsed with PBS supplemented with 0.5% BSA. Utilizing an Olympus FV1000 confocal laser microscope (Olympus Corporation, Japan), confocal images were obtained.

Western blot assay

HCC cells were collected and lysed with radio immunoprecipitation assay buffer (RIPA, Solarbio, China) prior to Western blot analysis. In order to ascertain the concentration of total cellular protein, a NanoDrop One UV spectrophotometer (Thermo Fisher Scientific, USA) was employed. Following that, protein samples were extracted utilizing a 10% PAGE gel rapid preparation kit (EpiZyme, China) and subsequently transferred onto a PVDF membrane (Milipore, Germany) with a pore size of 0.45 μm. The PVDF membrane was subsequently blocked at room temperature for two hours before being treated overnight at 4 °C with the diluted primary antibodies, followed by the designated secondary antibodies (Abcam, USA) for one hour. Enhanced chemiluminescence reagents (New Cell & Molecular Biotech, China) were employed to identify the bands. In order to quantify the data, Image J software (NIH Image, Bethesda, MD) was utilized. GAPDH (Absin, China), ERK and p-ERK (Proteintech, China), P38, p-P38, JNK and p-JNK (Abmart, China), ACYP2, KCNN4, and TERT (Abcam, UK) were the primary antibodies employed in this investigation.

Immunoprecipitation (IP) analysis

For immunoprecipitation (IP) analysis, cell lysates were obtained and subsequently subjected to protease inhibitor-containing lysis buffer. Immunoprecipitation was performed on cell extracts (2 mg/500 μL) utilizing the Pierce Co-immunoprecipitation Kit (Thermo Fisher Scientific, USA). Overnight at 4 °C, diluted cell lysates were combined with 2 to 5 μg of antibody and incubated. Following a 2-h rotation at 4 °C the following day, protein complexes were isolated utilizing magnetic protein A/G dynabeads. Following that, the samples were rinsed with wash buffer and boiled in preparation for Western blot analysis.

Enzyme-linked immunosorbent assay (ELISA)

The 96-well plates utilized in this enzyme-linked immunosorbent assay (ELISA) were loaded with 100 μL of samples or standards. The comprehensive methodology was carried out in accordance with the guidelines provided by the manufacturer (Sangon Biotech, China). The amount of TERT in each well was determined by calculating the absorbance at 450 nm using a microplate reader (Thermo Fisher Scientific, USA) and the corresponding standard curve.

Fluorescence in situ hybridization

For fluorescence in situ hybridization, 24-well plates were inoculated with the cells. In order to enhance cell permeability, the cells were fixated at an approximate confluence of 70%. Following that, the cells were subjected to treatment using probes (Ribobio, China) that contained either TERT or GAPDH in accordance with the guidelines provided in the fluorescence in situ hybridization kit (GenePharma, China). Following the staining of the cell nuclei with DAPI, the cells were examined via fluorescence microscopy.

Construction of nano-drug carrier

For the fabrication of nano-drug-carrier membranes derived from HCC cells, a PEI-loaded PLGA core was coated (PEI/NPs). Following this, a solution was prepared by combining 1 mL of aqueous NPs (10 mg/mL)

with 50 μL of PEI solution (10 mg/mL) and incubating at ambient temperature for 15 min. Following this, 500 μL of pcDNA-ACYP2 (500 ng/μL) was added to the mixture, and the mixture was incubated at ambient temperature for 20 min in order to produce pcDNA/PEI/NPs. Preparation of compounds comprising SK-Hep-1 cell vesicles and PEI nanoparticle complexes. The compounds were passed through 200 μm and 400 μm porous polycarbonate membranes by means of a micro-extruder (Avanti Polar Lipid). A total of ten extrusion cycles were utilized in order to generate pcDNA, PEI, and NPs@M.

(Loading rate: 0.25 mg plasmid/10 mg nanospheres = 2.5%. Encapsulation rate: according to the gel-blocking experiment, the encapsulation rate can reach 100%).

Animal experiments

Animal experiments were approved by the Animal Care and Ethical Committee of Nantong University. Every experimental procedure was conducted in strict adherence to the pertinent regulations and institutional protocols established by Nantong University. To generate stable expression cell lines for the HCC transplant tumor model, cells were transfected with pcDNA/PEI/NPs@M and its negative control (nc/PEI/NPs@M). Four weeks of age nude mice were injected subcutaneously with an estimated 1×10^7 cells, which were separated into left (nc/PEI/NPs@M) and right (pcDNA/PEI/NPs@M) axilla regions. The size of the tumor was assessed on a weekly basis utilizing calipers, and updates on tumor growth were documented accordingly. Subsequent to a duration of 3 weeks, the tumors were surgically removed from the rodents, and their mass and volume were documented. Moreover, sections of the lesions were prepared for H&E staining and immunohistochemistry analysis using paraffin-embedded techniques. To initiate the development of the orthotopic HCC mouse model, chloral hydrate was used to anesthetize nude BALB/c rodents. Following that, a surgical incision was made in the abdominal cavity, followed by the injection of 1×10^6 HCC cells into the designated area of the liver. After that, the abdomen was sealed. Every 7 days, saline, PEI/NPs@M, nc/PEI/NPs@M, and pcDNA/PEI/NPs@M were administered intravenously through the tail vein of nude rodents. Following this, experimental data were gathered on days 14, 21, and 28 utilizing the IVIS Spectrum (PerkinElmer, USA). In vitro studies: 100 μg/mL in cell culture. In vivo studies: in animal models, the dose of 10 mg/kg was administered intravenously.

Immunohistochemical staining

For immunohistochemical staining, paraffin-embedded sections were performed after the tumors were fixed in 4% paraformaldehyde. Subsequently, the tumor sections underwent antigen extraction via microwave irradiation after being defatted with xylene. Following that, the primary antibodies (H&E, PCNA, Ki67, Bcl-2, MMP2, ACYP2, and KCNN4) were incubated with the sections, which were then followed by the secondary antibodies (Santa Cruz, CA, USA). Following a comprehensive cleansing process, the sections underwent staining with 3,3′-diaminobenzidine (DAB) and hematoxylin. The sections were subsequently captured on film using an inverted microscope.

Statistical analysis

Statistical analysis was performed on the data utilizing SPSS 21.0 and GraphPad Prism Version 8.0. Using the chi-square test, the correlation between ACYP2 expression and clinicopathological characteristics of HCC was determined. A Kaplan–Meier survival analysis was employed to evaluate the overall survival rate. Consideration was given to a two-sided analysis with a significance level of 0.05 in order to ascertain statistical significance. The formula used to represent all data is mean ± standard deviation. In order to compare the groupings, either a t-test or analysis of variance was implemented.

Results

ACYP2 is lowly expressed in HCC

Four most dysregulated genes, namely ERCC5, ABCC2, ACYP2, and YTHDF2, were firstly identified by analyzing the Gene Expression Omnibus (GEO) dataset and filtering them from heatmaps and volcano maps. (Fig. 1A). QRT-PCR analyses further verified that the expression of ACYP2 was drastically downregulated ($p<0.001$) in HCC tissues relative to the adjacent normal tissues, whereas the expression of YTHDF2 was marginally overexpressed ($p<0.05$). Conversely, there were no noteworthy variations in the expression levels of ERCC5 and ABCC2 between the adjacent normal tissues and the HCC tissues (Fig. 1B). Furthermore, as indicated by the TCGA data, ACYP2 was the most significantly associated with the G-grade of patients diagnosed with HCC among the four dysregulated genes (Fig. S1A). Additionally, western blot analyses indicated a 50% reduction in the expression of the ACYP2 protein in HCC tissues relative to the neighboring normal tissues (Fig. 1C). As a result, ACYP2 was selected as an individual worthy of additional

scrutiny. Additionally, upon conducting a correlation analysis of clinicopathologic attributes, it was observed that the tumor size, tumor differentiation, and microvascular invasion (MVI) of patients with HCC were all significantly correlated with downregulated ACYP2 (Fig. 1D and Table S1). Furthermore, a receiver operating characteristic (ROC) curve was constructed, and its area under the curve was calculated to be 0.826. This value suggests that ACYP2, which was expressed at a low level, may possess diagnostic potential for hepatocellular carcinoma (Fig. 1E). Furthermore, according to both the TCGA data and follow-up of our enrolled cohort of HCC cases, the Kaplan–Meier survival analysis revealed that patients with low ACYP2 expression had a median survival time compared to high expression, with a significance level of $p = 0.0203$ (Fig. 1F and Fig. S1B). ACYP2 that is downregulated may collectively serve a crucial role in HCC.

ACYP2 inhibits HCC cell proliferation and metastasis

ACYP2 inhibits the proliferation and metastasis of HCC cells. The expression pattern of ACYP2 in HCC cell lines was analyzed in order to investigate its biological functions. To this end, pcDNA-ACYP2 and si-ACYP2-1/3, which are ACYP2-targeted RNA interference vectors and an overexpression vector, respectively, were constructed. The qRT-PCR analyses demonstrated that the levels of ACYP2 expression were significantly reduced in all five HCC cell lines compared to the liver normal cell line (LO2, Fig. 2A). Furthermore, it was observed that SMMC-7721 and BEL-7404 cells transfected with si-ACYP2-1 or si-ACYP2-2 exhibited significant transfection efficiencies, as did SK-Hep-1 cells transfected with pcDNA-ACYP2 (Fig. 2B). Subsequently, soft-agar colony formation and CCK-8 assays revealed that pcDNA-ACYP2-treated SK-Hep-1 cells exhibited a substantial inhibition in both colony-forming and cellular proliferation ($p < 0.05$). Conversely, SMMC-7721 and BEL-7404 cells treated with si-ACYP2-1 or si-ACYP2-2 exhibited a substantial enhancement in these parameters ($p < 0.05$) (Fig. 2C, Fig. S2B and Fig. S2C) Moreover, flow cytometry experiments demonstrated a significant increase in the number of SK-Hep-1 cells undergoing apoptosis when treated with pcDNA-ACYP2 ($p < 0.01$). Conversely, the number of SMMC-7721 and BEL-7404 cells that underwent apoptosis was drastically reduced when treated with either si-ACYP2-1 or si-ACYP2-2 (Fig. 2D and Fig. S2A). Furthermore, wound healing and transwell assays provided additional evidence [1] that pcDNA-ACYP2-treated SK-Hep-1 cells exhibited significantly diminished cell migration and invasion capabilities ($p < 0.001$), whereas si-ACYP2-1 or si-ACYP2-2-treated SMMC-7721 and BEL-7404 cells displayed conspicuous enhancements in these parameters ($p < 0.05$) (Fig. 2E, F). The cumulative results of these studies suggest that ACYP2 potentially functions as a tumor suppressor by impeding the proliferation and metastasis of HCC cells in vitro.

Cytoplasmic ACYP2 inhibits HCC progression through inactivating the KCNN4/ERK pathway

In order to obtain additional knowledge regarding the intracellular mechanisms of ACYP2 in HCC, a nucleoplasm separation assay was conducted. The presence of ACYP2 in both the nucleus and cytoplasm was identified in both normal (LO2) and HCC (SMMC-7721 and BEL-7404) cell lines via dual-localization. Furthermore, SK-Hep-1 cells that were treated with pcDNA-ACYP2 exhibited increased expression of ACYP2 in both the cytoplasm and nucleus (Fig. S3A). In addition to catalyzing the hydrolysis of phosphatase intermediates, ACYP2 decouples the Ca^{2+} and K^{+} channels across cellular membranes [19]. Furthermore, it has been demonstrated that ACYP2 influences Ca^{2+} concentration and is involved in the progression of glioma, whereas intracellular calcium can mobilize KCNN, a Ca^{2+}-dependent potassium channel. We therefore hypothesized that intracellular K^{+} homeostasis could be regulated via an interaction between ACYP2 and KCNN [8]. In line with findings reported in the literature, our qRT-PCR analyses revealed that the mRNA level of KCNN4 was the only one to decrease in SK-Hep-1 cells treated with pcDNA-ACYP2. This suggests that ACYP2 may play a regulatory role in the expression of KCNN4 in HCC (Fig.

(See figure on next page.)

Fig. 1 ACYP2 is lowly expressed in HCC. **A** The heatmap and volcano map analysis of the dysregulated genes in HCC from GEO database; **B** the expressions of 4 selected genes (ERCC5, ABCC2, ACYP2 and YTHDF2) in 52 HCC tissues and paired para-cancerous tissues were detected by qRT-PCR; **C** the protein expression of ACYP2 in HCC tissues and paired para-cancerous tissues was analyzed by western blot; **D** association analysis of ACYP2 expression with tumor differentiation, tumor size, and microvascular invasion of HCC cases; **E** ROC curve analysis of ACYP2 differentiating HCC from normal tissue; **F** Kaplan–Meier was used to assess the relationship between ACYP2 expression and the prognosis of HCC patients. $^{*}p < 0.05$, $^{**}p < 0.01$

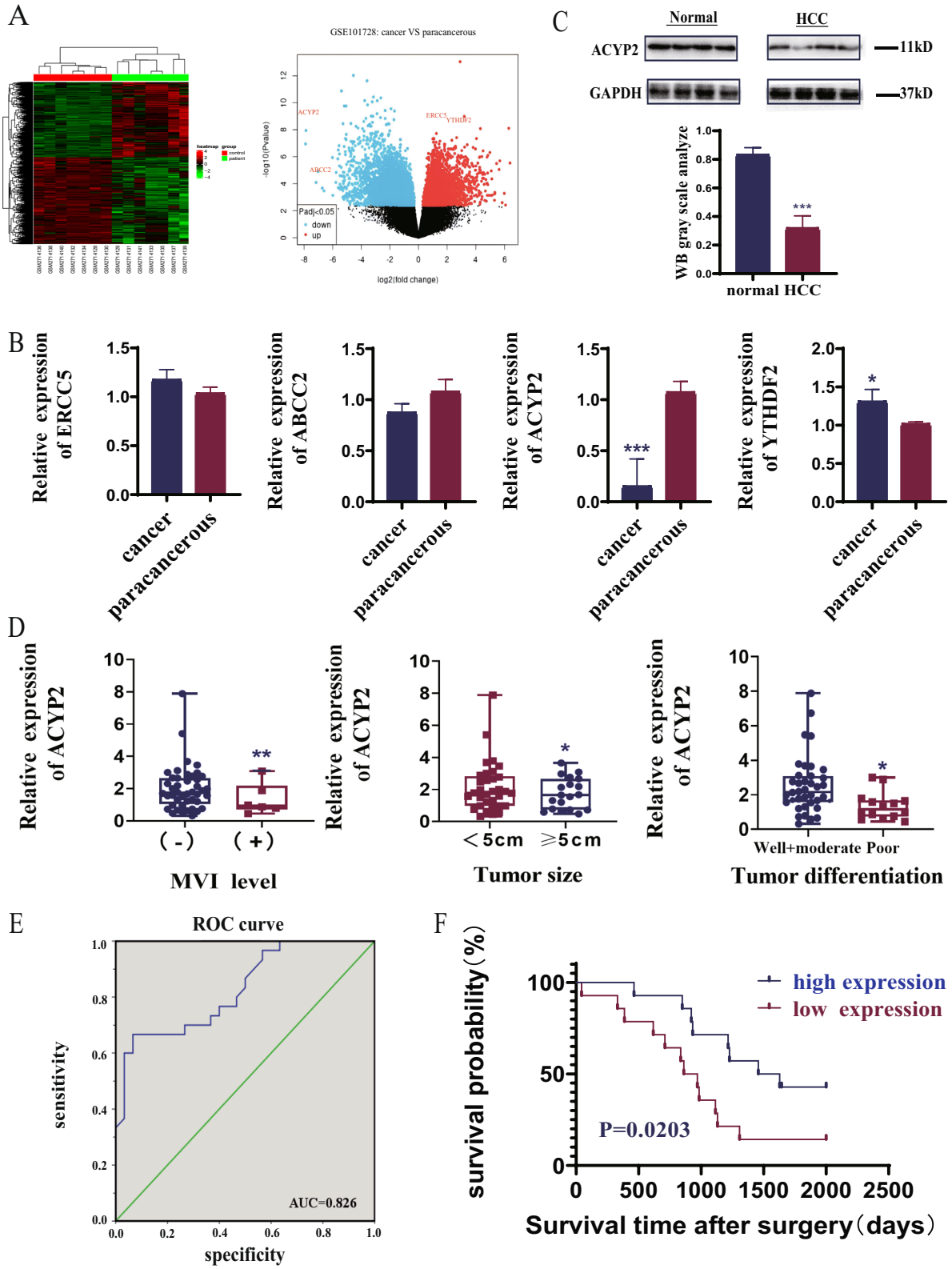

Fig. 1 (See legend on previous page.)

S3B). Furthermore, a negative correlation was observed between the expressions of KCNN4 and ACYP2 in HCC, as indicated by TCGA data (Fig. S3C). Additionally, qRT-PCR assays confirmed the overexpression of KCNN4 in HCC and found it to be negatively correlated with the expression of ACYP2 ($p < 0.01$) (Fig. 3A). Also, the cooperation between ACYP2 and KCNN4 was confirmed via co-IP experiments (Fig. 3B). In a similar fashion, qRT-PCR and western blotting were utilized to confirm their interaction at the molecular and protein levels; these techniques revealed that KCNN4 expression was upregulated subsequent to ACYP2 knockdown and downregulated subsequent to its overexpression (Fig. 3C, D). Following this, si-KCNN4 and si-KCNN4 + siACYP2 transfection efficiency assays were validated (Fig. S4A). Through recuperation experiments, the interaction between ACYP2 and KCNN4 was further clarified. As determined by the CCK-8, EDU, and soft agar colony formation assays, si-KCNN4 significantly inhibited the cell proliferation and colony-forming capabilities of SMMC-7721 and BEL-7404 cells. However, these characteristics were restored in cells treated with si-ACYP2 (si-ACYP2-1) + si-KCNN4 (Fig. 3E, Fig. S4B, D). Furthermore, flow cytometry analyses demonstrated a significant increase in the number of SMMC-7721 and BEL-7404 cells that underwent apoptosis when treated with si-KCNN4. Conversely, the number of SMMC-7721 and BEL-7404 cells that underwent apoptosis decreased drastically when treated with si-ACYP2 + si-KCNN4 (Fig. 3F and Fig. S4C). Additionally, wound healing and transwell assays demonstrated that si-KCNN4 significantly inhibited the migratory and invading capabilities of SMMC-7721 and BEL-7404 cells, whereas si-ACYP2 + si-KCNN4 significantly increased these functions in the aforementioned cells (Fig. 3G and Fig. S4E). In addition, ion-colorimetric analysis showed that both pcDNA-ACYP2-treated SK-Hep-1 and si-KCNN4-treated SMMC-7721 and BEL-7404 extracellular K^+ concentrations were significantly elevated, whereas si-ACYP2 + si-KCNN4-treated SMMC-7721 and BEL-7404 extracellular K^+ concentrations were significantly decreased (Fig. 3H and Fig. S4F). Subsequently, confocal fluorescence microscopy analysis revealed that the intracellular potassium fluorescence signals of SMMC-7721 and BEL-7404 cells treated with si-KCNN4 were significantly diminished, whereas they were reinstated to their initial levels in cells treated with si-ACYP2 + si-KCNN4 (Fig. 3I). By interacting with KCNN4, ACYP2 facilitates intracellular K^+ efflux, as demonstrated by these experiments.

It has been documented that KCNN4 influences the development of various types of cancer via the MAPK signaling pathway [20]. Additionally, a significant correlation was observed in the function of the downstream ACYP2 MAPK pathway according to KEGG data (Fig. S4G). Validation was performed on the signaling pathways of ERK, P38, and JNK and their phosphorylated proteins, which are essential for K^+ transport. The results of Western blot analysis revealed a substantial decrease in the expression levels of ERK and p-ERK in SMMC-7721 and BEL-7404 cells treated with si-KCNN4. Conversely, the expression levels of P38 and JNK remained unaltered. Furthermore, it was observed that si-ACYP2 + si-KCNN4-treated SMMC-7721 and BEL-7404 cells exhibited increased expression levels of both ERK and p-ERK, whereas pcDNA-ACYP2-treated SK-Hep-1 cells displayed decreased expression levels (Fig. 3J and Fig. S4H). By impeding the activation of KCNN4 and subsequent release of K^+, ACYP2 in HCC cells inhibits the ERK pathway and impedes the malignant progression of HCC.

Nuclear ACYP2 inhibits HCC progression and immortality through inactivating the TERT activity

As a telomere length-related gene, ACYP2 influences telomerase expression levels in addition to having its polymorphisms linked to the risk of multiple malignancies [21]. Additionally, by modulating telomerase activity, TERT affects telomere length, which impacts the prognosis and diagnosis of cancer. As a result, we postulated that the interaction between ACYP2 and TERT influences the length of telomeres [7]. To determine the mechanism by which ACYP2 and TERT function in the nucleus, the TCGA database was used to obtain HCC patient information. The correlation between ACYP2 and TERT expression levels were analyzed by Spearman correlation coefficient which correlation coefficient is

(See figure on next page.)

Fig. 2 ACYP2 inhibits HCC cell proliferation and metastasis in vitro. **A** The expression of ACYP2 in HCC cell lines was detected by qRT-PCR; **B** the transfection efficiencies of knockdown ACYP2 (si-ACYP2) and overexpression of ACYP2 (pcDNA-ACYP2) were measured by qRT-PCR; **C** the proliferation abilities of HCC cells treated with pcDNA-ACYP2 and si-ACYP2-1, -2 were analyzed by CCK-8 assay; **D** the apoptotic rates of HCC cells treated with pcDNA-ACYP2 and si-ACYP2-1, -2 were detected by flow cytometry; **E**, **F** the migration and invasion abilities of pcDNA-ACYP2 and si-ACYP2-1, -2 treated HCC cells were detected by wound healing and transwell methods. Scale bar: 200 μm; $^*p < 0.05$, $^{**}p < 0.01$, $^{***}p < 0.001$

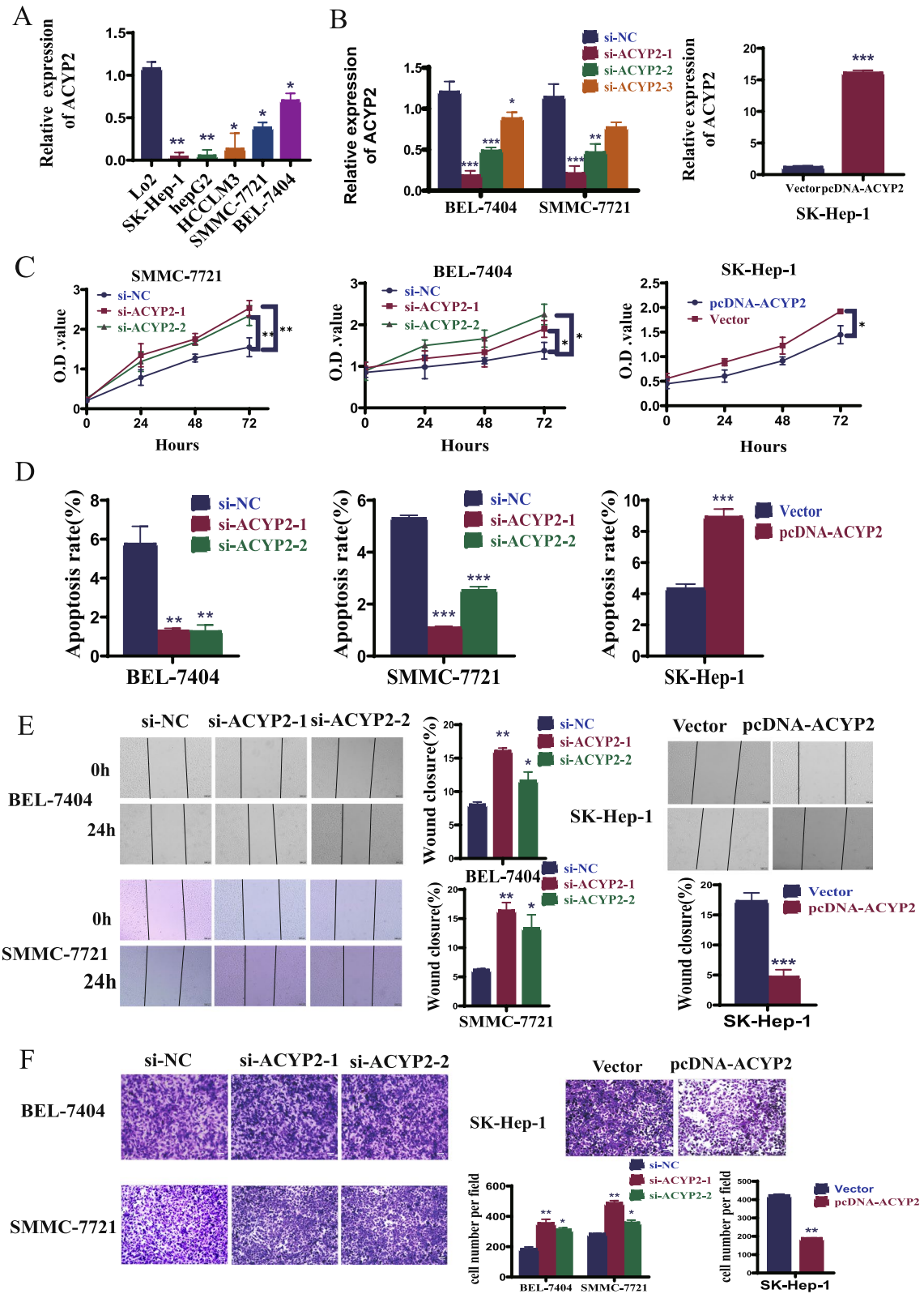

Fig. 2 (See legend on previous page.)

−0.15 ($p < 0.01$) (Fig. S3C). In addition, qRT-PCR assays confirmed that ACYP2 expression was negatively correlated with TERT overexpression in HCC (Fig. 4A). The interaction between ACYP2 and TERT was subsequently confirmed using a Co-IP assay (Fig. 4B). In a similar fashion, qRT-PCR and western blotting were utilized to confirm their interaction at the molecular and protein levels; these techniques revealed that the expression of TERT increased subsequent to ACYP2 suppression and decreased subsequent to its overexpression (Fig. 4C, D). The results of the enzyme immunoassay demonstrated that the level of TERT was considerably higher subsequent to the suppression of ACYP2, while it was considerably lower following its overexpression (Fig. 4E). Following this, si-TERT and si-TERT + si-ACYP2 constructs were fabricated and their transfection efficiencies were validated (Fig. S5A). By means of recuperation experiments, the relationship between ACYP2 and TERT was elaborated. The CCK-8, EDU, and soft agar colony formation assays provided evidence that si-TERT treatment substantially diminished the cell proliferation and colony-forming capabilities of SMMC-7721 and BEL-7404 cells. However, si-ACYP2 + si-TERT treatment restored these properties in SMMC-7721 and BEL-7404 cells (Fig. 4F, Fig. S5B, D). In the interim, wound healing and transwell assays demonstrated that si-TERT significantly inhibited the migratory and invading capabilities of SMMC-7721 and BEL-7404 cells, whereas si-ACYP2 + si-TERT-treated cells exhibited enhanced capabilities in these respects (Fig. 4G and Fig. S5E). Furthermore, flow cytometry experiments demonstrated a significant increase in the number of SMMC-7721 and BEL-7404 cells undergoing apoptosis when treated with si-TERT. Conversely, the number of SMMC-7721 and BEL-7404 cells undergoing apoptosis decreased drastically when treated with si-ACYP2 + si-TERT (Fig. 4H and Fig. S5C). The results of fluorescence in situ hybridization and qRT-PCR analysis revealed a notable decrease in telomere length in SMMC-7721 and BEL-7404 cells treated with si-TERT. Conversely, si-ACYP2 + si-TERT resulted in an increase in telomere length in these cells (Fig. 4I). Collectively, ACYP2 inhibits TERT in the nucleus, thereby reducing Telomere length (TL) and preventing HCC cells from surviving indefinitely.

Synthesis and identification of pcDNA/PEI/NPs@M nanocomposites

Identification and synthesis of pcDNA/PEI/NPs@M nanocomposites in light of the tumor suppressor function of ACYP2 in HCC, our objective was to utilize a vector that targets the delivery of ACYP2 as a possible therapeutic approach for HCC. Following encapsulation of the pcDNA-ACYP2 vector within PEI/NPs, the NPs were coated with HCC cell membranes (pcDNA/PEI/NPs@M). When analyzed using transmission electron microscopy (TEM), it was observed that pcDNA/PEI/NPs@M formed spherical vesicles that exhibited a consistent particle size distribution (Fig. 5A). Additionally, the zeta potential and grain size analyses revealed that the distances between nc/PEI/NPs@M and pcDNA/PEI/NPs@M were around 17.2 mV and 183.4 nm, and 16.5 mV and 241.7 nm, respectively. These results indicate that the NPs@M have the capability to serve as carriers for infiltration into the tumor tissues via the tumor vasculature wall (Fig. S6A). Furthermore, in order to evaluate the safety profile, PBS, pcDNA/PEI/NPs, PEI/NPs@M, and pcDNA/PEI/NPs@M labeled with Cy3 dye were synthesized. CCK-8 proliferation experiments revealed that both of these scaffolds exhibited minimal cytotoxicity towards SK-Hep-1 cells (Fig. 5B). Furthermore, flow cytometry analysis revealed that SK-Hep-1 cells exhibited remarkable uptake efficiencies for both Cy3/PEI/NPs@M and Cy3/pcDNA/PEI/NPs@M, while Cy3/pcDNA/PEI/NPs showed no uptake activity. The above results show that the nanomaterials encapsulating HCC cell membranes

(See figure on next page.)

Fig. 3 Cytoplasmic ACYP2 inhibits HCC progression through inactivating the KCNN4/ERK pathway. **A** KCNN4 expression was detected by qRT-PCR and correlation analysis its expression with ACYP2 in HCC; **B** the interaction between ACYP2 and KCNN4 was verified by Co-immunoprecipitation (IP) assay; **C** the mRNA expression of KCNN4 in si-ACYP2 (si-ACYP2-1) and pcDNA-ACYP2 treated HCC cells was detected by qRT-PCR; **D** the protein expression of KCNN4 in si-ACYP2 and pcDNA-ACYP2 treated HCC cells was detected by western blotting; **E** the proliferation abilities of HCC cells in si-NC, si-KCNN4 and si-ACYP2 + si-KCNN4 treatment groups were analyzed by CCK-8; **F** the apoptotic rates of HCC cells in si-NC, si-KCNN4 and si-ACYP2 + si-KCNN4 treatment groups were detected by flow cytometry; **G** the cell invasion abilities of si-NC, si-KCNN4 and si-ACYP2 + si-KCNN4 treatment groups were conducted by transwell assay; **H** the concentration of K^+ was detected by ion chromatography; **I** the fluorescence intensity of K^+ in HCC cells was measured by confocal fluorescence microscopy; **J** The expression of ERK, p-ERK, p38, p-p38, JNK and p-JNK proteins of si-NC, si-KCNN4 and si-ACYP2 + si-KCNN4 treatment groups were verified respectively by western blotting. Scale bar: 100 μm; $^*p < 0.05$, $^{**}p < 0.01$, $^{***}p < 0.001$

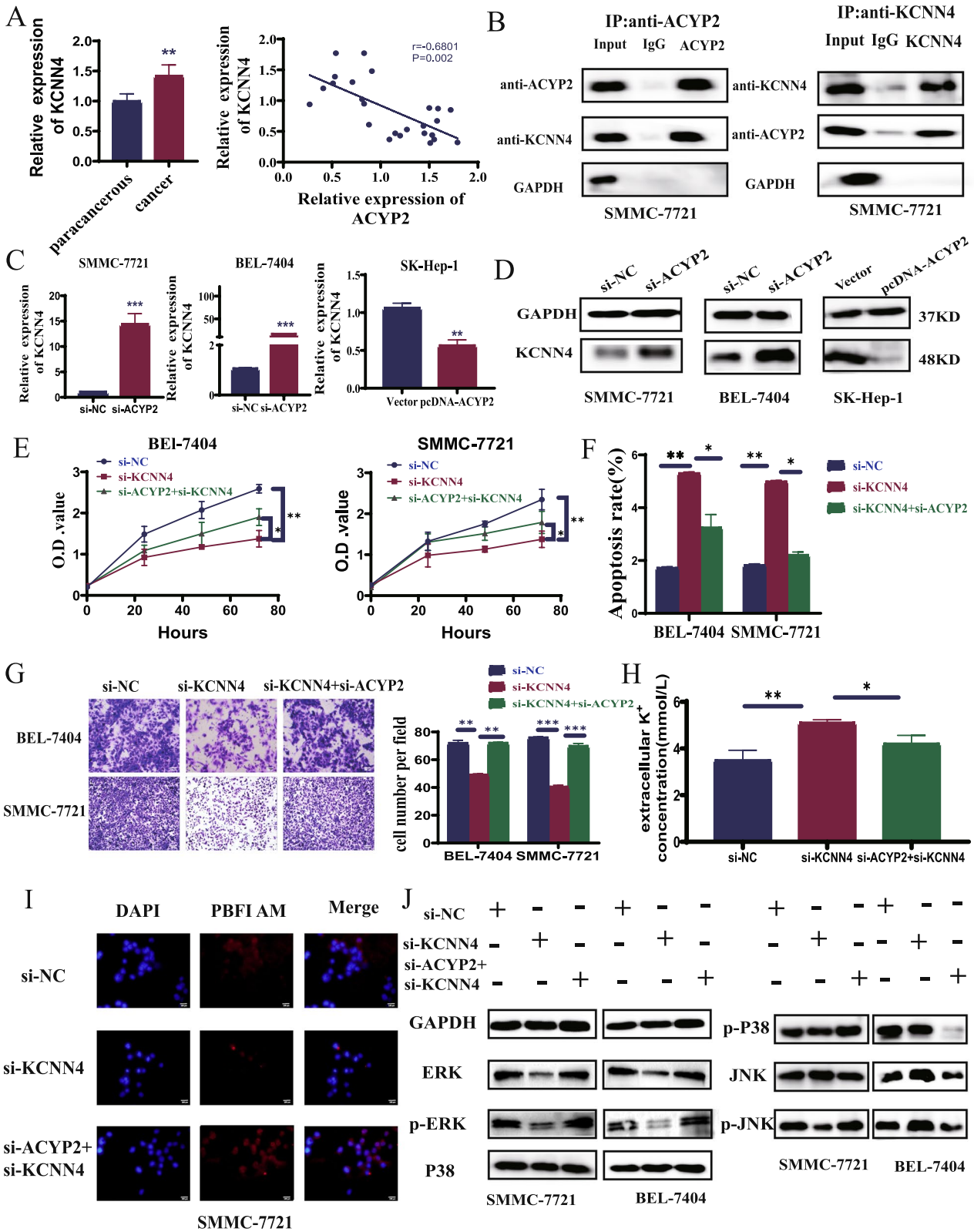

Fig. 3 (See legend on previous page.)

are better targeted (Fig. 5C). Following that, fluorescence imaging demonstrated that a greater concentration of Cy3/pcDNA/PEI/NPs@M nanocomposites was observed in the liver region. Furthermore, these nanocomposites exhibited a more proficient targeting capability compared to Cy3/pcDNA/PEI/NPs, thus exposing the HCC cell membrane's exceptional biocompatibility (Fig. 5D, E). In conclusion, pcDNA/PEI/NPs@M demonstrated exceptional safety and targeting capability in vivo.

Anti-tumor effects of pcDNA/PEI/NPs@M nanocomposites in subcutaneous graft tumor models

For subcutaneous tumor formation experiments involving nude mice, pcDNA/PEI/NPs@M transfected SK-Hep-1 cells were injected stably into the axilla. pcDNA/PEI/NPs@M could substantially inhibit the growth of subcutaneous tumors after 3 weeks of observation, the pcDNA/PEI/NPs@M treatment group exhibited a 50% reduction in tumor volume compared to the control group ($p < 0.001$) (Fig. 6A, B). In the pcDNA/PEI/NPs@M treatment group, tumor volume and weight were significantly reduced and rendered lighter in comparison to the negative vector group (Fig. 6C, D). Furthermore, the pcDNA/PEI/NPs@M treatment group exhibited a significantly decreased positive rate for Ki67 and PCNA (markers of tumor proliferation), Bcl-2 (marker of tumor apoptosis), and MMP2 (marker of tumor metastasis), as determined by H&E and immunohistochemical staining (Fig. 6E). Conversely, the rate of ACYP2 was significantly increased. Additionally, the pcDNA/PEI/NPs@M treatment group exhibited increased levels of ACYP2 protein and decreased levels of p-ERK and TERT proteins, similarly, increased levels of ACYP2 mRNA and decreased levels of KCNN4 and TERT mRNA, as determined by qRT-PCR and western blot assays (Fig. S7A, B). Furthermore, immunohistochemical analyses revealed a notable decrease in the expression of KCNN4 in the tissues of the group treated with pcDNA/PEI/NPs@M in comparison to the control group (Fig. S7C). Collectively, these results suggested that pcDNA/PEI/NPs@M inhibited the growth of HCC tumors in subcutaneous graft tumor models.

Anti-tumor effects of pcDNA/PEI/NPs@M nanocomposites in orthotopic HCC transplantation model

The objective of this study was to investigate the potential therapeutic effects of pcDNA/PEI/NPs@M nanocomposites on HCC. To achieve this, laparotomy was performed on nude mice, and SK-Hep-1 cells were injected into the liver of each mouse in order to establish an orthotopic HCC transplantation model. The mice were allocated arbitrarily into four groups and subsequently administered tail vein injections containing different types of substances: normal saline, PEI/NPs@M, nc/PEI/NPs@M, and pcDNA/PEI/NPs@M (Fig. 7A). Therefore, a significant reduction in fluorescence intensity was observed in the group of rodents treated with pcDNA/PEI/NPs@M at 7-day intervals, as compared to the remaining three groups (Fig. 7B, C). A concurrent and substantial decrease in both the quantity and mass of tumors was identified (Fig. 7D, E). Furthermore, the pcDNA/PEI/NPs@M treatment group exhibited decreased concentrations of aspartate aminotransferase (AST), alanine aminotransferase (ALT), alkaline phosphatase (ALP), and creatinine (Cr) when compared to the other groups. However, there were no abnormalities detected in total protein (TP), albumin (ALB), globulin (GLB), and urea nitrogen (BUN) (Fig. S8A-H). In the interim, western blot and qRT-PCR analyses revealed that pcDNA/PEI/NPs@M treatment increased the expression of ACYP2 while decreasing the expression of KCNN4 and TERT in tumor tissues (Fig. 7F–I). In conclusion, the enzyme correlation immunoassay demonstrated that the administration of pcDNA/PEI/NPs@M resulted in a reduction in the concentration of TERT in tumor tissues when compared to the three groups that came before it (Fig. 7J). Altogether, pcDNA/PEI/NPs@M has a relatively high therapeutic effect on HCC.

Immunohistochemical analysis demonstrated a substantial decrease in tumor proliferation and metastasis

(See figure on next page.)

Fig. 4 Nuclear ACYP2 inhibits HCC progression and immortality through inactivating the TERT activity. **A** TERT expression was detected by qRT-PCR and correlation analysis its expression with ACYP2 in HCC; **B** the interaction between ACYP2 and TERT was verified by Co-IP; **C** the mRNA expression of TERT in si-ACYP2 and pcDNA-ACYP2 treated HCC cells was detected by qRT-PCR; **D** the protein expression of TERT in si-ACYP2 and pcDNA-ACYP2 treated HCC cells was verified by western blotting; **E** the concentration of TERT in si-ACYP2 and pcDNA-ACYP2 treated HCC cells was analyzed by enzyme-linked immunoassay; **F** the proliferation abilities of HCC cells in si-NC, si-TERT and si-ACYP2 + si-TERT treatment groups were analyzed by CCK-8; **G** the cell invasion abilities of si-NC, si-TERT and si-ACYP2 + si-TERT treatment groups were detected by transwell assay; **H** the apoptostic rates of si-NC, si-TERT and si-ACYP2 + si-TERT cells treatment groups were detected by flow cytometry. **I** The changes of telomere length in si-NC, si-TERT and si-ACYP2 + si-TERT treatment groups were observed by fluorescence in situ hybridization and qRT-PCR. Scale bar: 100 μm; $^{*}p < 0.05$, $^{**}p < 0.01$, $^{***}p < 0.001$

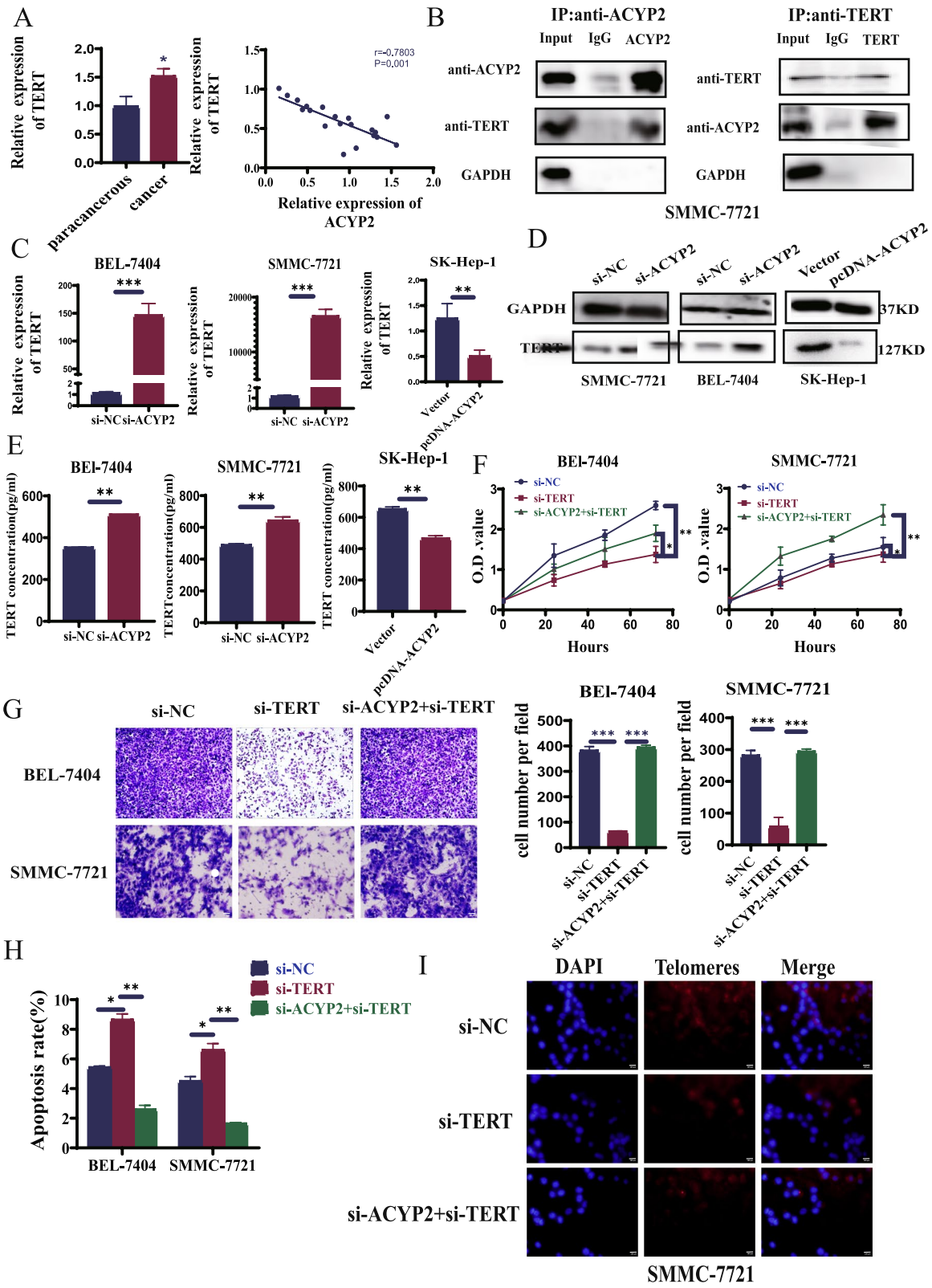

Fig. 4 (See legend on previous page.)

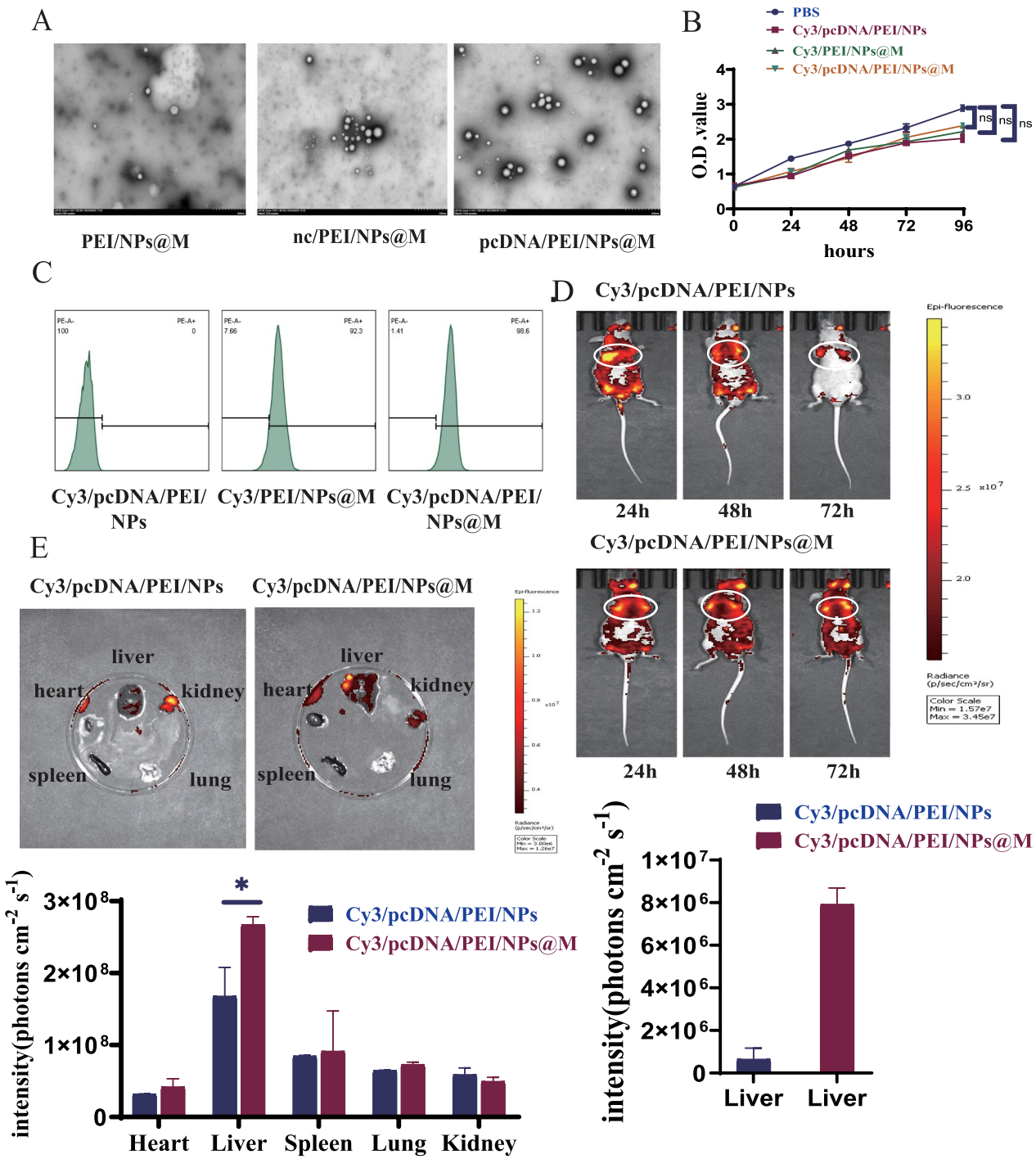

Fig. 5 Synthesis and identification of pcDNA/PEI/NPs@M nanocomposites. **A** The structures of PEI/NPs@M, nc/PEI/NPs@M and pcDNA/PEI/NPs@M were observed by transmission electron microscopy (TEM); **B** the cytotoxicity of PBS, Cy3/pcDNA/PEI/NPs, Cy3/PEI/NPs@M and Cy3/pcDNA/PEI/NPs@M complexes was tested using CCK-8 assay; **C** the particle uptake efficiencies of Cy3/pcDNA/PEI/NPs, Cy3/PEI/NPs@M and Cy3/pcDNA/PEI/NPs@M complex were measured by flow cytometry; **D**, **E** fluorescence imaging revealed that more Cy3/pcDNA/PEI/NPs@M nanocomposites were concentrated in the liver area, and their targeting ability was more superior than that of Cy3/pcDNA/PEI/NPs. ns, non-significant, $^{*}p < 0.05$

within the pcDNA/PEI/NPs@M treatment group (Fig. 8A) whereas apoptosis was conspicuously augmented. Following H&E staining, the pcDNA/PEI/NPs@M treatment group exhibited lung, spleen, and heart tissues that were normal in appearance, devoid of substantial necrosis (Fig. 8B). pcDNA/PEI/NPs@M inhibited the proliferation and metastasis of HCC cells in orthotopic HCC transplantation model. And there were no obvious nodules and necrosis in the organs of mice, indicating that the nanoparticles encapsulated in tumor cell membranes were not organ toxic.

Discussion

HCC is an extremely lethal malignant tumor of the liver. Research has been dedicated to understanding the pathogenesis, early diagnosis, treatment, and prognosis of this malignant tumor [22–25]. Owing to inadequate rates of early detection, the majority of HCC patients are diagnosed once the disease has advanced to a point where surgical intervention is no longer viable [23, 26]. Consequently, chemotherapy has emerged as a prevalent therapeutic approach for patients with advanced HCC [27]. Nevertheless, despite its high propensity for drug resistance, HCC remains a highly resistant malignancy [28]. Therefore, further analysis of the pathogenesis of HCC and search for new diagnostic and therapeutic targets are of certain significance for the prognosis and survival of HCC patients.

The expression of ACYP2 has been observed exclusively in metastatic colorectal cancer cells in humans, which implies a potential association with metastatic characteristics [29]. Its precise function in human malignancies, including HCC, remains unknown. We present compelling evidence in this study that ACYP2 functions as a tumor suppressor gene in HCC. Initially, we established a statistically significant association between diminished ACYP2 expression and poorer survival in HCC patients, as well as demonstrated that ACYP2 expression is substantially reduced in HCC tissues relative to control groups. Furthermore, ACYP2 inhibition induced cell apoptosis and substantially enhanced cell proliferation, colony formation, migration and invasion in HCC cells.

Prior to delving deeper into the intracellular mechanism of ACYP2 in HCC, we established that ACYP2 exhibits a dual localization pattern, occurring simultaneously in the nucleus and cytoplasm. The hydrolysis of phosphatase intermediates and the decoupling of Ca^{2+} and K^+ channels across the cell membrane are both processes facilitated by ACYP2. Also, ACYP2 has been proved to be implicated in cancer progression in gliomas by affecting Ca^{2+} concentration, whereas the potassium-calcium-activated channel subfamily N (KCNN) serves as a Ca^{2+} dependent potassium channel which can be mobilized by intracellular calcium [30]. Among them, KCNN4 has been extensively researched in a diverse array of physiological processes, including immunomodulation, cell proliferation, and apoptosis [31, 32]. In addition, it has been found to promote a malignant phenotype in cancer cells by regulating invasion and metastasis in many types of cancer [9, 33]. For example, KCNN4 is highly expressed in triple-negative breast cancer that has been found to promote migration and EMT of triple-negative breast cancer cells [34]. In clear cell renal carcinoma, high expression of KCNN4 is associated with low survival and a high likelihood of metastasis [35]. High expression of KCNN4 is associated with lower survival in patients with pancreatic cancer [36], and KCNN4 is overexpressed in proximal tumors compared to distal tumors of colorectal cancer [37]. Therefore, we hypothesized that ACYP2 in the cytoplasm leads to K^+ efflux by interacting with KCNN4. This hypothesis was additionally corroborated in this investigation through the observation that KCNN4 knockdown resulted in upregulation of ACYP2 expression, which inhibits K^+ efflux. Furthermore, ACYP2 knockdown was capable of reversing the inhibitory impact of KCNN4 knockdown on cellular proliferation and migration. Additionally, it has been reported that KCNN4 modulates the progression of multiple malignancies via the MAPK signaling pathway. ERK is frequently observed in human cancers, such as HCC, where its expression regulates invasion, migration, apoptosis, and cell proliferation [38, 39]. Our findings indicate that ACYP2 in cytoplasm inhibits KCNN4 activation and subsequent K^+ release, thereby interfering with the ERK pathway and impeding the malignant progression of HCC.

(See figure on next page.)

Fig. 6 Anti-tumor effects of pcDNA/PEI/NPs@M nanocomposites in subcutaneous graft tumor models. **A** Image of nude mice inoculated with nc/PEI/NPs@M and pcDNA/PEI/NPs@M treated HCC cells on left and right sides of armpit for 21 days, respectively; **B** images of subcutaneous tumors in nude mice after surgical dissection; **C** tumor growth volume and weight measurements of the tumors in nude mice; **D** 21-day growth curve of tumor in nude mice was drawn; **E** the expressions of Ki67, PCNA, Bcl-2, MMP2 (biomarkers of tumor proliferation, apoptosis and metastasis) and ACYP2 in subcutaneous tumors were detected by H&E and IHC staining. Scale bar: 200 μm; $^*p < 0.05$, $^{**}p < 0.01$

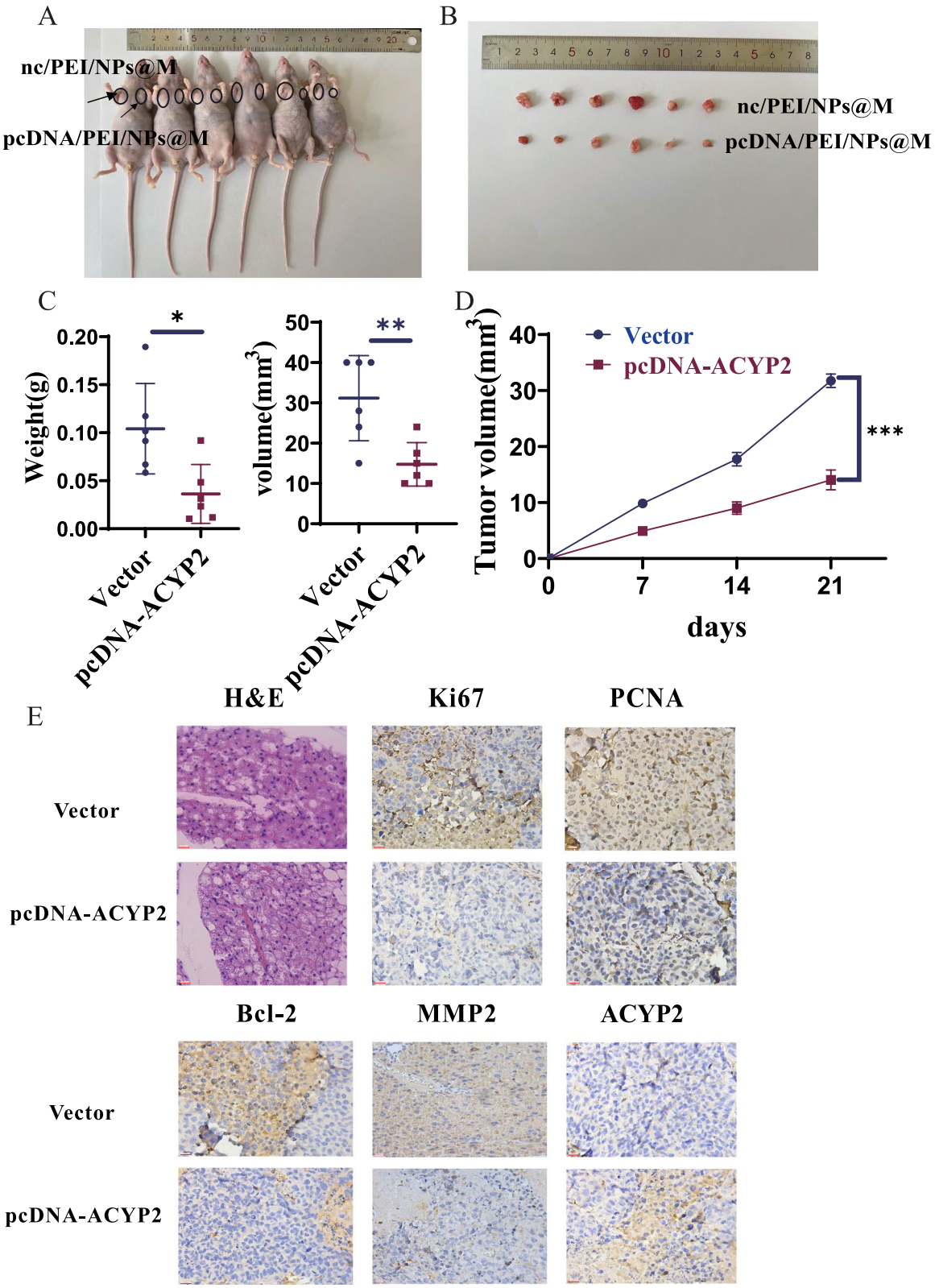

Fig. 6 (See legend on previous page.)

TERT plays a pivotal role in the initiation of cancer, ensuring genomic stability by preserving telomere length and enabling cells to evade senescence [40]. By means of telomere-dependent or independent mechanisms, the telomerase complex is crucial in the development of cancer [41]. These complexes are specific to cancer at the level of individual cells and tissue types [42]. TERT is influenced by a range of genetic and epigenetic modifications that impact telomerase activity within tumors [43]. The telomerase activity expressed via TERT influences the length of telomeres and can serve as a valuable marker for the diagnosis and prognosis of diverse types of cancer [44–46]. It was found that ACYP2 in nucleus inhibited TERT activity through down-regulation of TERT expression, which resulted in shortening of chromosome telomere length, inhibiting cell immortality and hindering HCC progression, but the specific mechanism of ACYP2's interaction with TERT needs to be further investigated.

Further research is required in order to comprehensively comprehend the potential therapeutic benefits of ACYP2 in HCC. Alternative methods include non-viral vector-mediated gene transfer, which is favored due to its exceptional biological safety and diminished likelihood of eliciting an adverse immune response, as well as integration into the host virus gene to facilitate efficient gene delivery [47]. The immunogenicity of non-viral vectors is comparatively low in comparison to viral vectors. However, their clinical applicability is constrained by the low efficiency of transfection [48]. As a result, additional endeavors are required to create non-viral vectors that are not contagious but exhibit enhanced security. As research advances, an increasing number of non-viral vectors are being developed and investigated, with particular emphasis on the utilization and advancement of drug delivery systems associated with nanotechnology. These developments have yielded noteworthy progress, thereby fostering further investigation and application in this domain [49, 50]. NPs, in particular, are extensively employed in the fabrication of gene drug delivery systems due to their exceptional chemical and physical characteristics [51]. NPs are frequently unable to advance to the clinical stage as a result of their toxicity and degradation. PEI and its derivatives, which function as cationic polymers designed for the delivery of nucleic acids, find extensive application in fundamental research and serve as benchmark agents within the domain of polymer-based gene delivery [16]. Consequently, PEI was employed in conjunction with NPs to enhance the efficacy of the action. In the course of our investigation, pcDNA vectors encapsulated in tumor cell membranes encased PEI/NPs vectors to generate pcDNA/PEI/NPs@M. According to our findings, pcDNA/PEI/NPs@M accumulates significantly in HCC cells but has minimal impact on the lungs, spleen, and heart of rodents in orthotopic mouse models. More importantly, pcDNA/PEI/NPs@M demonstrated favorable therapeutic effects in both subcutaneous graft tumor models and orthotopic mouse models by effectively inhibiting tumor growth in nude mice, resulting in a significant reduction in both tumor weight and quantity. As a result, ACYP2 could potentially be targeted therapeutically in patients with HCC. In the future, we will study the cell membrane-encapsulated nanomaterials more intensively, and strive to realize the simultaneous targeting of ACYP2, KCNN4 and TERT for better therapeutic efficacy.

Taken together, our current study demonstrates that lowly expressed ACYP2 acts as a tumor suppressor, which can inhibit HCC progression through its dual roles in the cytoplasm and nucleus of HCC cells. That is, cytoplasmic ACYP2 inhibits K^+ efflux and ERK pathway by interacting with KCNN4 to impede the malignant progression of HCC; Nuclear ACYP2 impedes the progression of HCC by inhibiting the activity of TERT, leading to shortening of telomere length and inhibiting cellular immortalization. Moreover, pcDNA/PEI/NPs@M represents a promising targeted nano-therapeutic strategy for HCC. Thus, this study provides a new direction for exploring the mechanisms in hepatocarcinogenesis and a novel therapeutic target for this deadly disease.

(See figure on next page.)

Fig. 7 Anti-tumor effects of pcDNA/PEI/NPs@M nanocomposites in orthotopic HCC transplantation model. **A** Schematic diagram of in situ treatment; **B**, **C** the fluorescence intensity of nude mice HCC cells injected with saline, PEI/NPs@M, nc/PEI/NPs@M and pcDNA/PEI/NPs@M, was respectively detected by in vivo imaging; **D**, **E** tumor weight and number were respectively measured in mice after surgical dissection; **F**–**H** the expressions of ACYP2, KCNN4 and TERT in tumor tissues treated with saline, PEI/NPs@M, nc/PEI/NPs@M and pcDNA/PEI/NPs@M were detected by qRT-PCR, respectively; **I** the expressions of KCNN4 and TERT in tumor tissues treated with pcDNA/PEI/NPs@M were detected by western blotting; **J** the concentration of TERT in saline, PEI/NPs@M, nc/PEI/NPs@M and pcDNA/PEI/NPs@M was observed by enzyme-linked immunoassay. ns, non-significant, $^{**}p < 0.01$, $^{***}p < 0.001$

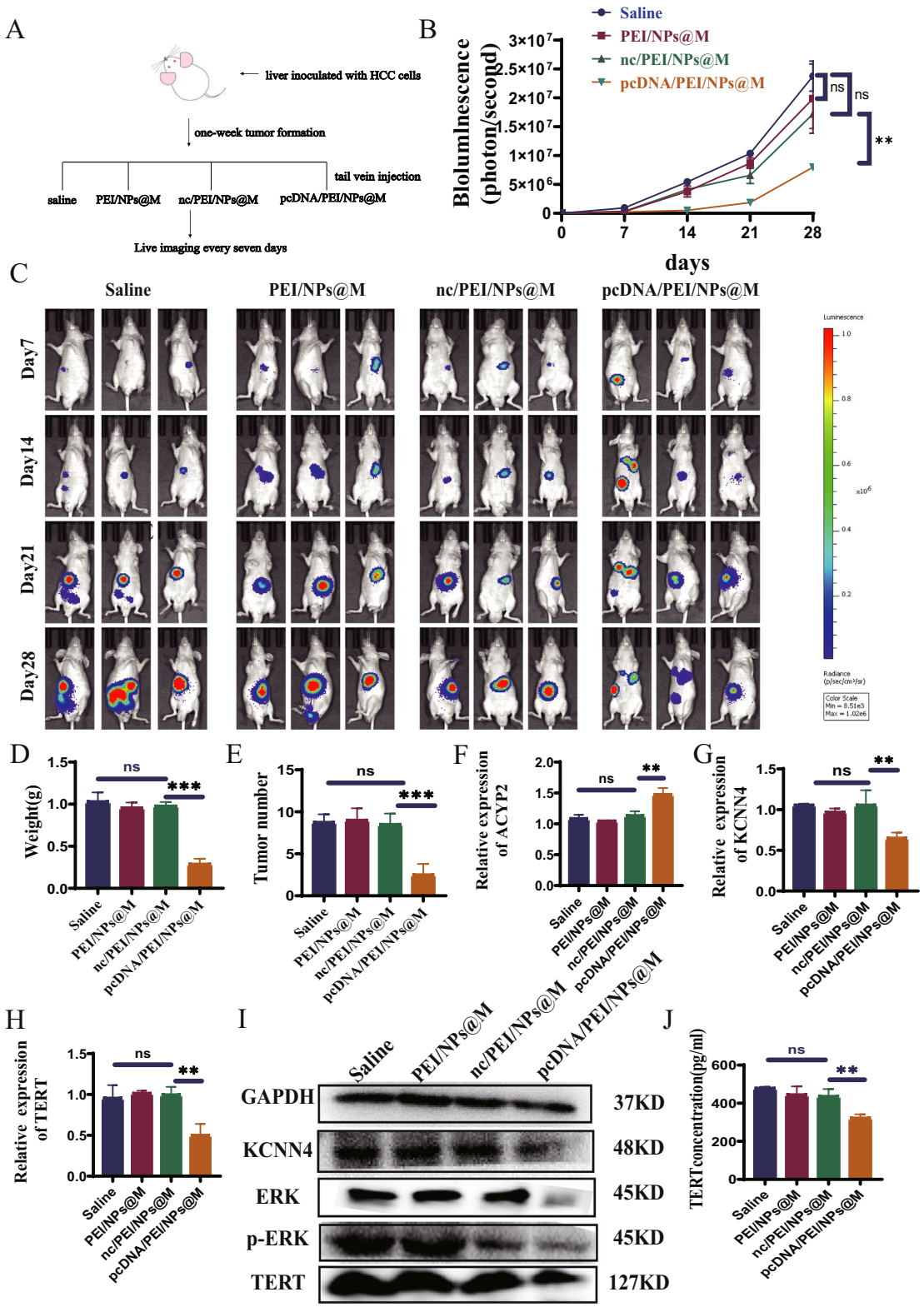

Fig. 7 (See legend on previous page.)

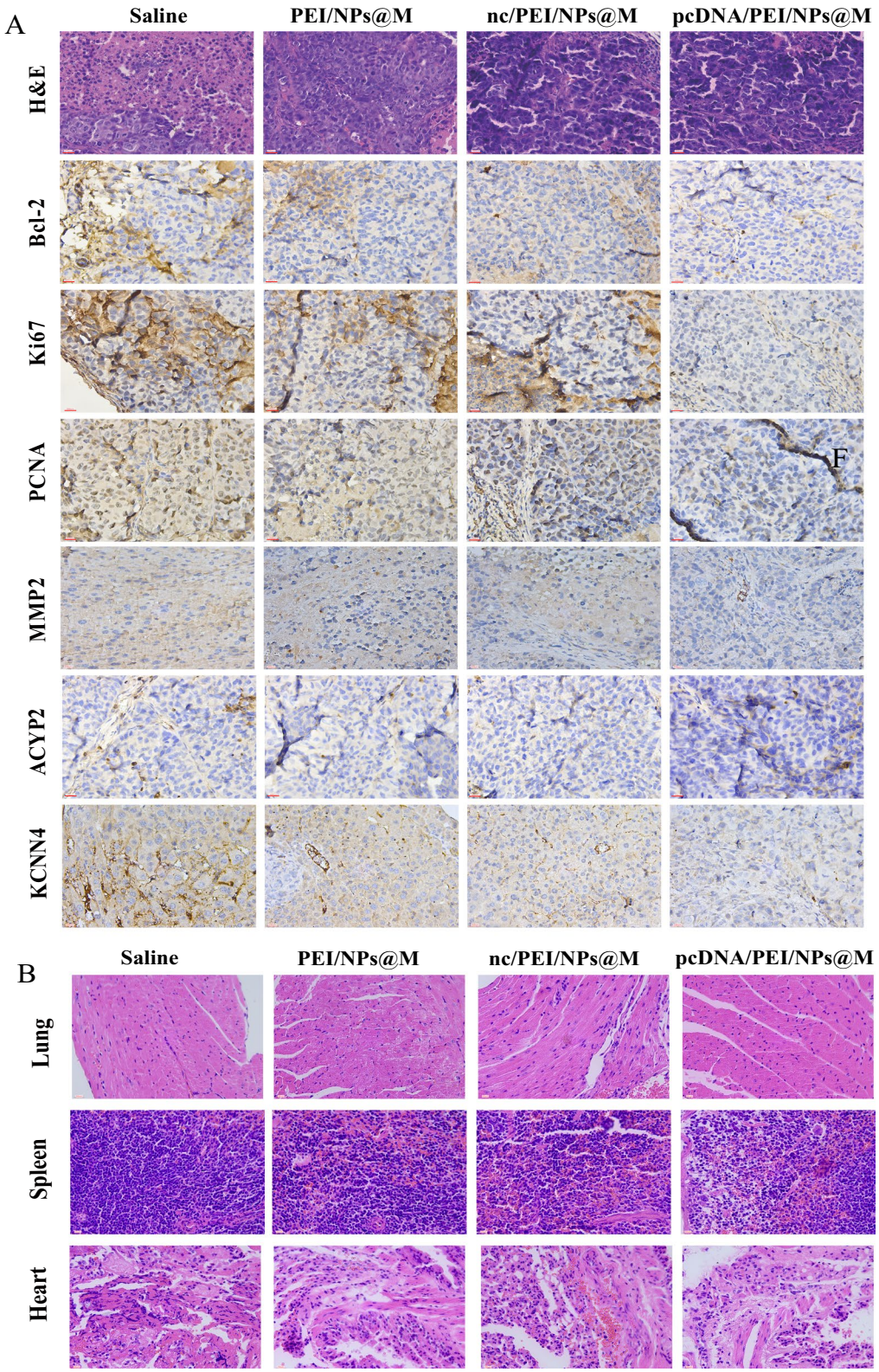

Fig. 8 pcDNA/PEI/NPs@M impacts on related protein in transplanted tumors. **A** IHC analyses the expressions of Ki67, PCNA, MMP2, Bcl-2, KCNN4 and ACYP2 on the tumors of nude mice after injection of saline, PEI/NPs@M, nc/PEI/NPs@M and pcDNA/PEI/NPs@M, respectively; **B** H&E staining to investigate the lung, spleen and heart tissues of nude mice after injection of saline, PEI/NPs@M, nc/PEI/NPs@M and pcDNA/PEI/NPs@M, respectively. Scale bar: 200 μm

Supplementary Information

The online version contains supplementary material available at https://doi.org/10.1186/s12951-024-02827-4.

Supplementary Material 1.

Acknowledgements
A special thanks for the Clinical Research Center of Affiliated Hospital of Nantong University and the School of Medicine of Nantong University for the support of this study.

Author contributions
Y.W. and H.B. wrote the paper. J.W. and B.C. contributed to summarize clinical advances of Tumor marker. J.X and K.J. provided insightful discussions and comments on the manuscript. C.L., G.Z. and F.W. revised the manuscript and led the project. All authors reviewed the manuscript.

Funding
This work was financially supported by the National Natural Science Foundation of China (81873978), Postdoctoral Research Funding Project of Jiangsu Province (2021K012A), Project of Science and Technology Bureau in Nantong City (JC2023108), Jiangsu Provincial Research Hospital (YJXYY202204-ZD06).

Data availability
No datasets were generated or analysed during the current study.

Declarations

Ethics approval and consent to participate
The ethics committee of the Affiliated Hospital of Nantong University approved this research, and informed consent was obtained from all participants.

Competing interests
The authors declare no competing interests.

Author details
[1]Research Center of Clinical Medicine, Affiliated Hospital of Nantong University, Medical School of Nantong University, Nantong 226001, China. [2]Department of Laboratory Medicine, Affiliated Hospital of Nantong University, Medical School of Nantong University, Nantong 226001, China. [3]Nantong Institute of Liver Diseases, Nantong Third People's Hospital Affiliated Nantong Hospital 3 of Nantong University, Nantong 226006, China. [4]Division of Life Science, The Hong Kong University of Science and Technology, Clear Water Bay, Kowloon, Hong Kong, SAR 999077, China.

Received: 25 April 2024 Accepted: 31 August 2024
Published online: 12 September 2024

References

1. Liang Y, Li J, Xu H, Pang M, Hu C, Weng X, Xie W. Cepharanthine suppresses proliferation and metastasis and enhances apoptosis by regulating JAK2/Stat3 pathway in hepatocellular carcinoma. Cell Mol Biol. 2023;69(14):94–100. https://doi.org/10.14715/cmb/2023.69.14.15.
2. Sadagopan N, He AR. Recent progress in systemic therapy for advanced hepatocellular carcinoma. Int J Mol Sci. 2024;25(2):1259. https://doi.org/10.3390/ijms25021259.
3. Martínez-Rodríguez S, Cámara-Artigas A, Gavira JA. First 3-D structural evidence of a native-like intertwined dimer in the acylphosphatase family. Biochem Biophys Res Commun. 2023;682:85–90. https://doi.org/10.1016/j.bbrc.2023.09.053.
4. Wang S, Zhou L, Ji N, Sun C, Sun L, Sun J, Du Y, Zhang N, Li Y, Liu W, Lu W. Targeting ACYP1-mediated glycolysis reverses lenvatinib resistance and restricts hepatocellular carcinoma progression. Drug Resist Updat. 2023;69: 100976. https://doi.org/10.1016/j.drup.2023.100976.
5. Sakano Y, Noda T, Kobayashi S, Kitagawa A, Iwagami Y, Yamada D, et al. Clinical significance of acylphosphatase 1 expression in combined HCC-iCCA, HCC, and iCCA. Dig Dis Sci. 2022;67(8):3817–30. https://doi.org/10.1007/s10620-021-07266-x.
6. Chang X, Yang Z, Wang H, Wang Y, Li J, Zhang Y, Teng Z, Han Z. ACPY2 gene polymorphisms on cancer risk: a systematic review and meta-analysis. Nucleosides Nucleotides Nucleic Acids. 2022;41(11):1205–23. https://doi.org/10.1080/15257770.2022.2096899.
7. Gentiluomo M, Capurso G, Morelli L, Ermini S, Pasquali C, Latiano A, et al. Genetically determined telomere length is associated with pancreatic neuroendocrine neoplasms onset. Neuroendocrinology. 2022;112(12):1168–76. https://doi.org/10.1159/000524659.
8. Li M, Ruan B, Wei J, Yang Q, Chen M, Ji M, Hou P. ACYP2 contributes to malignant progression of glioma through promoting Ca^{2+} efflux and subsequently activating c-Myc and STAT3 signals. J Exp Clin Cancer Res. 2020;39(1):106. https://doi.org/10.1186/s13046-020-01607-w.
9. Chen S, Su X, Mo Z. KCNN4 is a potential biomarker for predicting cancer prognosis and an essential molecule that remodels various components in the tumor microenvironment: a pan-cancer study. Front Mol Biosci. 2022;9: 812815. https://doi.org/10.3389/fmolb.2022.812815.
10. Nam YW, Downey M, Rahman MA, Cui M, Zhang M. Channelopathy of small- and intermediate-conductance Ca^{2+}-activated K^+ channels. Acta Pharmacol Sin. 2023;44(2):259–67. https://doi.org/10.1038/s41401-022-00935-1.
11. Jiang Y, Fan M, Yang Z, Liu X, Xu Z, Liu S, et al. Recent advances in nanotechnology approaches for non-viral gene therapy. Biomater Sci. 2022;10(24):6862–92. https://doi.org/10.1039/d2bm01001a.
12. Huang Y, Huang B, Ye D, Luo X, Xiong X, Xiong H, Wang H, Zou Q, Liang J, Wang S, Wu L. Nano-induced endothelial leakiness-reversing nanoparticles for targeting, penetration and restoration of endothelial cell barrier. Acta Biomater. 2024;175:226–39. https://doi.org/10.1016/j.actbio.2023.12.040.
13. Gharoonpour A, Simiyari D, Yousefzadeh A, Badragheh F, Rahmati M. Autophagy modulation in breast cancer utilizing nanomaterials and nanoparticles. Front Oncol. 2023;13:1150492. https://doi.org/10.3389/fonc.2023.1150492.
14. Chou PY, Lin SY, Wu YN, Shen CY, Sheu MT, Ho HO. Glycosylation of OVA antigen-loaded PLGA nanoparticles enhances DC-targeting for cancer vaccination. J Control Release. 2022;351:970–88. https://doi.org/10.1016/j.jconrel.2022.10.002.
15. Meher MK, Unnikrishnan BS, Tripathi DK, Packirisamy G, Poluri KM. Baicalin functionalized PEI-heparin carbon dots as cancer theranostic agent. Int J Biol Macromol. 2023;253(Pt 3): 126846. https://doi.org/10.1016/j.ijbiomac.2023.126846.
16. Casper J, Schenk SH, Parhizkar E, Detampel P, Dehshahri A, Huwyler J. Polyethylenimine (PEI) in gene therapy: current status and clinical applications. J Control Release. 2023;362:667–91. https://doi.org/10.1016/j.jconrel.2023.09.001.
17. Zhou YL, Yang QQ, Yan YY, Zhu C, Zhang L, Tang JB. Localized delivery of miRNAs targets cyclooxygenases and reduces flexor tendon adhesions. Acta Biomater. 2018;70:237–48. https://doi.org/10.1016/j.actbio.2018.01.047.
18. Scully MA, Sterin EH, Day ES. Membrane-wrapped nanoparticles for nucleic acid delivery. Biomater Sci. 2022;10(16):4378–91. https://doi.org/10.1039/d2bm00447j.
19. Nassi P, Marchetti E, Nediani C, Liguri G, Ramponi G. Acylphosphatase induced modifications in the functional properties of erythrocyte membrane sodium pump. Biochim Biophys Acta. 1993;1147(1):19–26. https://doi.org/10.1016/0005-2736(93)90311-m.
20. Hausmann D, Hoffmann DC, Venkataramani V, Jung E, Horschitz S, Tetzlaff SK, et al. Autonomous rhythmic activity in glioma networks drives brain tumour growth. Nature. 2023;613(7942):179–86. https://doi.org/10.1038/s41586-022-05520-4.
21. Huang P, Li R, Shen L, He W, Chen S, Dong Y, Ma J, Chen X, Xu M. Single nucleotide polymorphisms in telomere length-related genes are associated with hepatocellular carcinoma risk in the Chinese Han population. Ther Adv Med Oncol. 2020;12:1758835920933029. https://doi.org/10.1177/1758835920933029.
22. Rui T, Zhang X, Guo J, Xiang A, Tang N, Liu J, Mao Z. Serum-exosome-derived miRNAs serve as promising biomarkers for HCC diagnosis. Cancers. 2022;15(1):205. https://doi.org/10.3390/cancers15010205.

23. Li Y, Xiong H. Correlation of LAGE3 with unfavorable prognosis and promoting tumor development in HCC via PI3K/AKT/mTOR and Ras/RAF/MAPK pathways. BMC Cancer. 2022;22(1):298. https://doi.org/10.1186/s12885-022-09398-3.
24. Sultan MQ, Charfeddine B, Hussain Al-Salih AR. Evaluation of the diagnostic performance of alpha-1-antitrypsin in early detection of hepatocellular carcinoma. Cell Mol Biol. 2023;69(14):177–85. https://doi.org/10.14715/cmb/2023.69.14.29.
25. Lumkul L, Jantaree P, Jaisamak K, Wongkummool W, Lapisatepun W, Orrapin S, Udomruk S, Lo Piccolo L, Chaiyawat P. Combinatorial gene expression profiling of serum HULC, HOTAIR, and UCA1 lncRNAs to differentiate hepatocellular carcinoma from liver diseases: a systematic review and meta-analysis. Int J Mol Sci. 2024;25(2):1258. https://doi.org/10.3390/ijms25021258.
26. Chakraborty E, Sarkar D. Emerging therapies for hepatocellular carcinoma (HCC). Cancers. 2022;14(11):2798. https://doi.org/10.3390/cancers14112798.
27. Köstek O, Demirel A, Hacıoğlu MB, Tastekin D, Karabulut S, Gündogdu A, et al. The prognostic factors in patients with advanced hepatocellular carcinoma: impact of treatment sequencing. J Chemother. 2024. https://doi.org/10.1080/1120009x.2024.2305066.
28. Ladd AD, Duarte S, Sahin I, Zarrinpar A. Mechanisms of drug resistance in HCC. Hepatology. 2023. https://doi.org/10.1097/hep.0000000000000237.
29. Zhou L, Fu Z, Wang S, Jia J, Cheng Y, Zheng Y, Zhang N, Lu W, Yao Z. ACYP1 is a pancancer prognostic indicator and affects the immune microenvironment in LIHC. Front Oncol. 2022;12: 875097. https://doi.org/10.3389/fonc.2022.875097.
30. Nikitin ES, Postnikova TY, Proskurina EY, Borodinova AA, Ivanova V, Roshchin MV, Smirnova MP, Kelmanson I, Belousov VV, Balaban PM, Zaitsev AV. Overexpression of KCNN4 channels in principal neurons produces an anti-seizure effect without reducing their coding ability. Gene Ther. 2023. https://doi.org/10.1038/s41434-023-00427-9.
31. Mo X, Zhang CF, Xu P, Ding M, Ma ZJ, Sun Q, et al. KCNN4-mediated Ca(2+)/MET/AKT axis is promising for targeted therapy of pancreatic ductal adenocarcinoma. Acta Pharmacol Sin. 2022;43(3):735–46. https://doi.org/10.1038/s41401-021-00688-3.
32. Ran L, Ye T, Erbs E, Ehl S, Spassky N, Sumara I, Zhang Z, Ricci R. KCNN4 links PIEZO-dependent mechanotransduction to NLRP3 inflammasome activation. Sci Immunol. 2023;8(90): eadf4699. https://doi.org/10.1126/sciimmunol.adf4699.
33. Zuccolini P, Barbieri R, Sbrana F, Picco C, Gavazzo P, Pusch M. IK channel-independent effects of clotrimazole and senicapoc on cancer cells viability and migration. Int J Mol Sci. 2023;24(22):16285. https://doi.org/10.3390/ijms242216285.
34. Li M, Tian P, Zhao Q, Ma X, Zhang Y. Potassium channels: novel targets for tumor diagnosis and chemoresistance. Front Oncol. 2022;12:1074469. https://doi.org/10.3389/fonc.2022.1074469.
35. Cui Y, Shen T, Xu F, Zhang J, Wang Y, Wu J, et al. KCNN4 may weaken antitumor immune response via raising Tregs and diminishing resting mast cells in clear cell renal cell carcinoma. Cancer Cell Int. 2022;22(1):211. https://doi.org/10.1186/s12935-022-02626-7.
36. Soret B, Hense J, Lüdtke S, Thale I, Schwab A, Düfer M. Pancreatic $K_{Ca}^{3.1}$ channels in health and disease. Biol Chem. 2023;404(4):339–53. https://doi.org/10.1515/hsz-2022-0232.
37. Song Y, Deng Z, Sun H, Zhao Y, Zhao R, Cheng J, Huang Q. Predicting tumor repopulation through the gene panel derived from radiation resistant colorectal cancer cells. J Transl Med. 2023;21(1):390. https://doi.org/10.1186/s12967-023-04260-x.
38. Saleem S. Targeting MAPK signaling: a promising approach for treating inflammatory lung disease. Pathol Res Pract. 2024;254: 155122. https://doi.org/10.1016/j.prp.2024.155122.
39. Jiang H, Liao J, Wang L, Jin C, Mo J, Xiang S. The multikinase inhibitor axitinib in the treatment of advanced hepatocellular carcinoma: the current clinical applications and the molecular mechanisms. Front Immunol. 2023;14:1163967. https://doi.org/10.3389/fimmu.2023.1163967.
40. Liu M, Zhang Y, Jian Y, Gu L, Zhang D, Zhou H, Wang Y, Xu ZX. The regulations of telomerase reverse transcriptase (TERT) in cancer. Cell Death Dis. 2024;15(1):90. https://doi.org/10.1038/s41419-024-06454-7.
41. Zhang Y, Hou K, Tong J, Zhang H, Xiong M, Liu J, Jia S. The altered functions of shelterin components in ALT cells. Int J Mol Sci. 2023;24(23):16830. https://doi.org/10.3390/ijms242316830.
42. Kumar N, Sethi G. Telomerase and hallmarks of cancer: an intricate interplay governing cancer cell evolution. Cancer Lett. 2023;578: 216459. https://doi.org/10.1016/j.canlet.2023.216459.
43. Taheri M, Ghafouri-Fard S, Najafi S, Kallenbach J, Keramatfar E, Atri Roozbahani G, Heidari Horestani M, Hussen BM, Baniahmad A. Hormonal regulation of telomerase activity and hTERT expression in steroid-regulated tissues and cancer. Cancer Cell Int. 2022;22(1):258. https://doi.org/10.1186/s12935-022-02678-9.
44. Hasanau TN, Pisarev EP, Kisil OV, Zvereva ME. The TERT promoter: a key player in the fight for cancer cell immortality. Biochemistry. 2023;88(Suppl 1):S21–38. https://doi.org/10.1134/s000629792314002x.
45. Alimohamadi M, Larijani A, Pour-Rashidi A, Farzin M, Ebrahimi H, Rahmani M, Hendi K, Yarandi KK, Aghajanian S, Shirani M. Comparative analysis of the prognostic significance of IDH, TERT, EGFR and MGMT status in patients with adult non-H3-altered grade 4 gliomas: a prospective cohort study. World Neurosurg. 2024;181:e628–39. https://doi.org/10.1016/j.wneu.2023.10.102.
46. Lyu SI, Popp FC, Simon AG, Schultheis AM, Zander T, Fretter C, Schröder W, Bruns CJ, Schmidt T, Quaas A, Knipper K. Copy-number-gain of telomerase reverse transcriptase (hTERT) is associated with an unfavorable prognosis in esophageal adenocarcinoma. Sci Rep. 2023;13(1):17699. https://doi.org/10.1038/s41598-023-44844-7.
47. Dogbey DM, Torres VES, Fajemisin E, Mpondo L, Ngwenya T, Akinrinmade OA, Perriman AW, Barth S. Technological advances in the use of viral and non-viral vectors for delivering genetic and non-genetic cargos for cancer therapy. Drug Deliv Transl Res. 2023;13(11):2719–38. https://doi.org/10.1007/s13346-023-01362-3.
48. Spunde K, Korotkaja K, Zajakina A. Recombinant viral vectors for therapeutic programming of tumour microenvironment: advantages and limitations. Biomedicines. 2022;10(9):2142. https://doi.org/10.3390/biomedicines10092142.
49. Liu G, Li J, Wang X, He R, Zhang Y. An activatable dual polymer nanosystem for photoimmunotherapy and metabolic modulation of deep-seated tumors. Adv Healthc Mater. 2024;13: e2303305. https://doi.org/10.1002/adhm.202303305.
50. Farzipour S, Jalali Zefrei F, Bahadorikhalili S, Alvandi M, Salari A, Shaghaghi Z. Nanotechnology utilizing ferroptosis inducers in cancer treatment. Anti-cancer Agents Med Chem. 2024. https://doi.org/10.2174/0118715206278427231215111526.
51. Ijaz M, Aslam B, Hasan I, Ullah Z, Roy S, Guo B. Cell membrane-coated biomimetic nanomedicines: productive cancer theranostic tools. Biomater Sci. 2024. https://doi.org/10.1039/d3bm01552a.

Publisher's Note